ACS chemical biology

Letters

pubs.acs.org/acschemicalbiology

Quadruplex-Flanking Stem Structures Modulate the Stability and Metal Ion Preferences of RNA Mimics of GFP

Eman A. Ageely,[†,§] Zachary J. Kartje,[†,§] Kushal J. Rohilla,[‡,§] Christopher L. Barkau,[‡] and Keith T. Gagnon*[,†,‡]

[†]Department of Chemistry and Biochemistry, Southern Illinois University, Carbondale, Illinois 62901, United States

[‡]Department of Biochemistry and Molecular Biology, Southern Illinois University, School of Medicine, Carbondale, Illinois 62901, United States

Supporting Information

ABSTRACT: The spinach family of RNA aptamers are RNA mimics of green fluorescent protein (GFP) that have previously been designed to address the challenges of imaging RNA inside living cells. However, relatively low levels of free intracellular magnesium limited the practical use of these aptamers. Recent cell-based selections identified the broccoli RNA aptamer, which requires less magnesium for fluorescence, but the basis for magnesium preference remained unclear. Here, we find that the broccoli RNA structure is very similar to that of baby spinach, a truncated version of the spinach aptamer. Differences in stability and metal ion preferences between these two aptamers, and among broccoli mutants, are primarily associated with the sequence and structure of predicted quadruplex-flanking stem structures. Mutation of purine−purine pairs in broccoli at the terminal stem−quadruplex transition caused reversion of broccoli to a higher magnesium dependence. Unique duplex-to-quadruplex transitions in GFP-mimic RNAs likely explain their sensitivity to magnesium for stability and fluorescence. Thus, optimizations designed to improve aptamers should take into consideration the role of metal ions in stabilizing the transitions and interactions between independently folding RNA structural motifs.

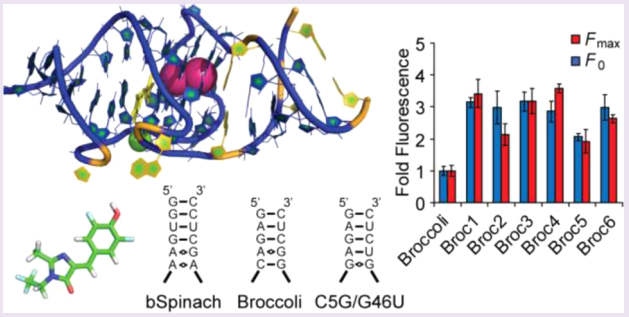

RNAs known as aptamers can be systematically evolved and selected to bind small molecules with high affinity and specificity.[1,2] Aptamers that bind fluorescent molecules can be used for visualizing RNA in synthetic biology applications, metabolite sensing, or monitoring dynamics inside living cells.[3−8] The unique three-dimensional structure of an aptamer confers its specificity and affinity for ligands, while positive counterions neutralize the negatively charged phosphate backbone to facilitate folding and stability.[9,10] Specific metal ions, such as magnesium and potassium, often bridge tertiary structures via hydrogen bonding networks and site-specific binding.[10−12] Thus, understanding the structure, stability, and metal ion interactions of aptamers promises to offer critical insight into their activity and design.

Fluorescent RNA aptamers have faced a number of challenges to their practical use as molecular tags for imaging RNA inside of cells. Early generation aptamers suffered from high background fluorescence and toxicity inside of cells, as well as low quantum yields.[13,14] More recently, RNA aptamers were selected to bind and activate fluorescence of chemically modified versions of HBI [(Z)-4-(4-hydroxybenzylidene)-1,2-dimethyl-1H-imidazol-5(4H)-one], the fluorophore that is generated within green fluorescent protein (GFP).[15] From these *in vitro* selections, the "spinach" RNA aptamer was identified, which fluoresces green similar to GFP. Additional versions of spinach, such as spinach2 (higher thermal stability) and baby spinach (minimal size), have been subsequently developed.[7,16] Diverse HBI fluorophore versions have also been reported, such as DFHBI-1T [(Z)-4-(3,5-difluoro-4-hydroxybenzylidene)-2-methyl-1-(2,2,2-trifluoroethyl)-1H-imidazol-5(4H)-one)] (Figure 1A), which shifts the excitation and emission spectrum to better match that of GFP.[17] Despite low cellular toxicity, reduced background fluorescence, and relatively high quantum yields, a requirement for non-physiological levels of magnesium has complicated the use of spinach aptamers inside of cells.

To overcome magnesium requirements and low thermodynamic stability, new selections were developed using cell-based selection and directed evolution.[18] These selections resulted in "broccoli," an RNA aptamer that binds DFHBI-1T, possesses greater thermal stability in the presence of reduced magnesium, and is only 49 nucleotides, approximately the size of baby spinach. Our interest in using broccoli as a fluorescent tag for imaging RNA in living cells prompted us to investigate its structure and function. We reasoned that broccoli RNA structure was similar to that of the spinach RNA aptamers

Received: January 15, 2016
Accepted: July 28, 2016

DOI: 10.1021/acschembio.6b00047
ACS Chem. Biol. XXXX, XXX, XXX−XXX

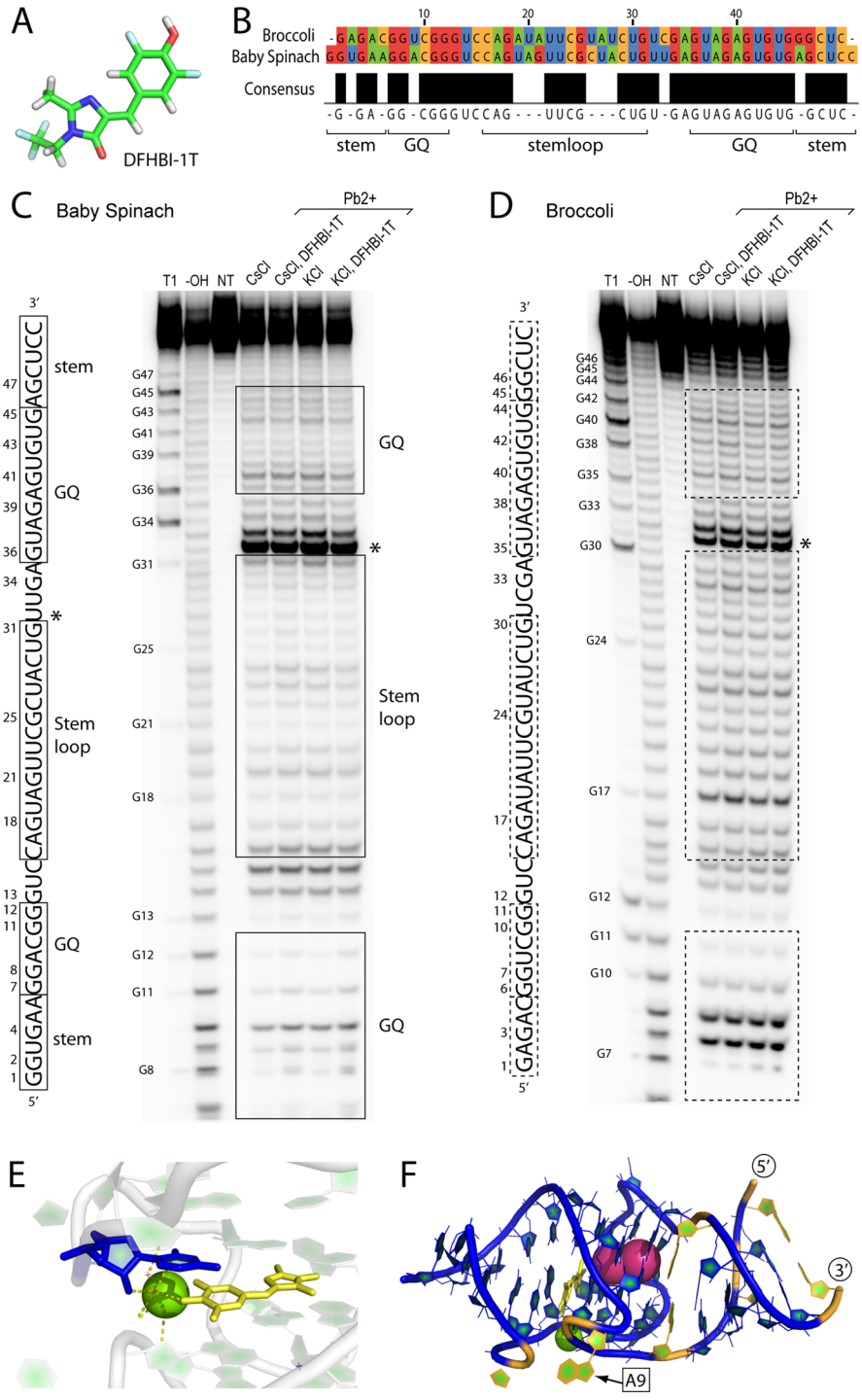

Figure 1. Sequence and structural comparisons support a strong similarity between baby spinach and broccoli RNA aptamers. (A) Structure of DFHBI-1T, the small molecule that is bound and fluorescently activated by baby spinach and broccoli aptamers. (B) Sequence alignment of broccoli and baby spinach RNAs. The consensus sequence is shown, and secondary structure alignment predicted from the spinach aptamer structure[16] (PDB ID: 4TS2) is indicated below. (C,D) Lead cleavage mapping of baby spinach and broccoli RNA structures. The sequence is shown to the left and labeled with structural alignment from the spinach aptamer structure[16] as well as nucleotide numbering. Lead cleavage mapping is shown, and the treatments for each lane are indicated above the gel. Bands on the gel that correspond to nucleotides in the sequence (shown to the left) are boxed. An asterisk indicates the base where magnesium ion binding is implicated. GQ, G-quadruplex; T1, T1 RNase cleavage ladder; −OH, alkaline hydrolysis ladder; NT, no treatment; Pb2+, addition of lead acetate. (E) Uridine U61 of spinach (blue), which corresponds to U32 of baby spinach,[16] is hydrogen-bonded to a water molecule coordinated by a magnesium ion (green), which also stabilizes DFHBI-1T (yellow) binding. (F) A fragment of the spinach RNA aptamer crystal structure[16] is shown that corresponds to the shared consensus sequence with baby spinach. Nucleotides that are identical between baby spinach and broccoli are shown in blue, whereas the few nucleotides that are different are shown in orange. A9, the only base found within the consensus quadruplex that differs between baby spinach and broccoli, is indicated. DFHBI-1T is shown in yellow. Potassium ions are shown as magenta spheres and coordinated magnesium ion as a green sphere.

DOI: 10.1021/acschembio.6b00047
ACS Chem. Biol. XXXX, XXX, XXX−XXX

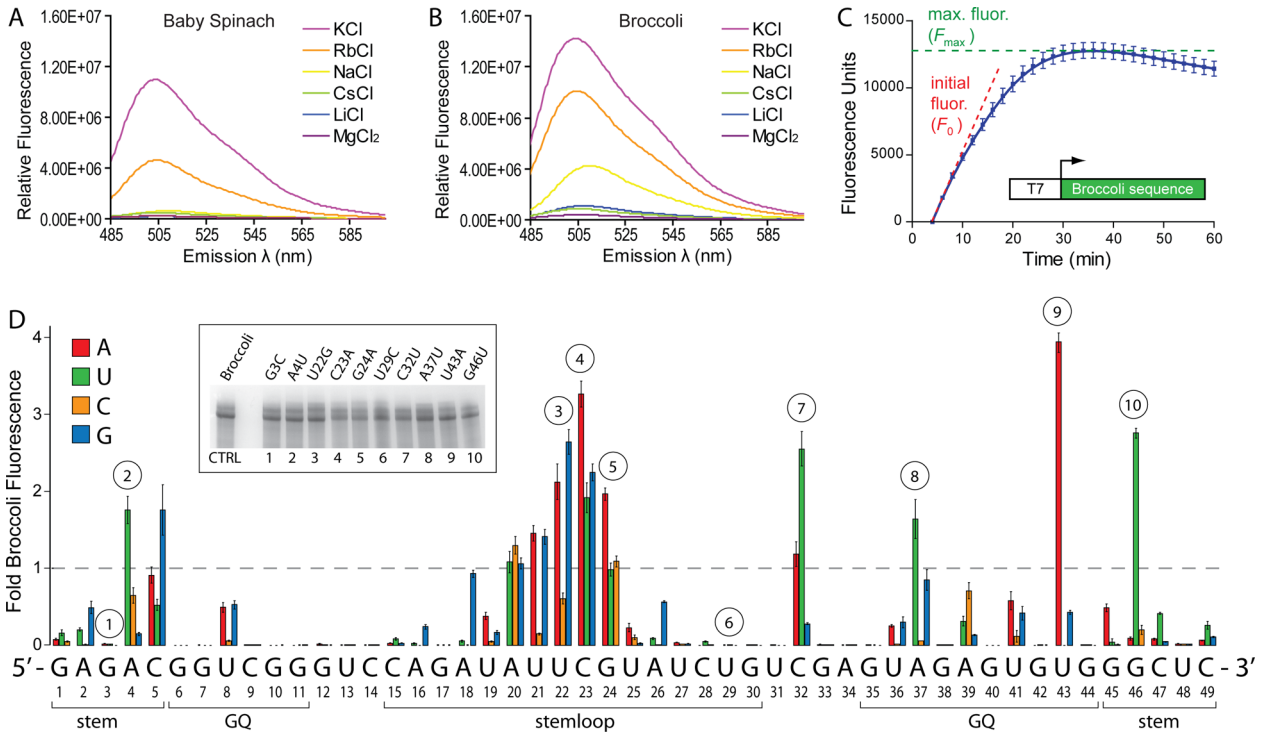

Figure 2. Metal-ion-dependent fluorescence and mutagenesis suggest the presence of a G-quadruplex and stem structures within broccoli RNA. Fluorescence emission is plotted for baby spinach (A) and broccoli (B) RNA aptamers in buffered solution containing DFHBI-1T and the indicated salts. (C) Example data for broccoli RNA using a transcription-based mutagenesis screen. T7 promoter DNA sequence is fused upstream of the broccoli sequence and used for *in vitro* transcription reactions containing the DFHBI-1T fluorophore. Initial fluorescence (F_0) and maximum fluorescence (F_{max}) are taken to approximate the relative folding and fluorescence activity of broccoli RNA concurrently with RNA synthesis. (D) Fluorescence results from systematic mutagenesis of broccoli RNA. Every nucleotide was individually substituted with one of three other nucleotides and fluorescence activity measured. Normalized activity of control broccoli RNA fluorescence is indicated by a dashed light gray line. Only F_{max} is plotted. Broccoli RNA sequence and nucleotide numbering are indicated below. Putative structures are indicated below and based upon the spinach crystal structure[16] and sequence alignment between broccoli and baby spinach. Mutant broccoli RNA reactions chosen for subsequent gel analysis (inset) by denaturing gel electrophoresis are indicated by circled numbers. Error bars are standard deviation from three separate analyses.

and in particular that it contains a G-quadruplex, considering that (1) it was selected using essentially the same fluorophore molecule that spinach activates, (2) spinach contains a G-quadruplex structure that binds DFHBI, (3) another fluorescent RNA aptamer that binds an HBI derivative was shown to have nuclear magnetic resonance chemical shifts indicative of G-quadruplexes, (4) a dependence for potassium ions was previously reported for spinach RNA fluorescence, and (5) broccoli contains a disproportionately high guanine to cytosine nucleotide ratio of 2:1.[16,18,19] In addition, simple alignment of the broccoli sequence with baby spinach sequence revealed high similarity (Figure 1B). Using the crystal structure of spinach as a guide,[16] the nucleotides that form its quadruplex core are nearly a perfect consensus between baby spinach and broccoli, with only a single A to U conversion at one position. Thus, we hypothesized that differences between broccoli and baby spinach fluorescence, magnesium preference, and stability likely arise from structural differences outside a quadruplex core.

To experimentally probe the structure of baby spinach and broccoli, we performed limited cleavage with lead acetate.[20] Lead is a divalent metal ion that accelerates phosphodiester bond cleavage. Cleavage correlates with regions of flexibility and accessibility within an RNA structure.[21,22] Both baby spinach and broccoli RNAs were refolded in the absence or presence of DFHBI-1T and either cesium chloride or potassium chloride. Potassium is known to stabilize G-quadruplexes by specific binding while cesium does not. We found no significant differences in the lead cleavage pattern of baby spinach or broccoli across these conditions (Figure 1C,D). However, overall lead cleavage patterns appeared quite similar between baby spinach and broccoli. These results suggest that large structural changes do not occur in the presence of potassium or DFHBI-1T and that baby spinach and broccoli possess similar structures.

Lead acetate is known to cause very strong phosphodiester bond cleavage at divalent metal ion binding sites within RNA structures,[21−23] thus acting as a specific probe for metal ion coordination. In agreement with this phenomenon, we observed excessive cleavage at the 3′ phosphodiester bond of uridine 32 (U32) in baby spinach, which corresponds to the same uridine in the spinach crystal structure that makes direct polar contact with a magnesium-coordinated water molecule via its 2′ hydroxyl (Figure 1E). This magnesium ion binds tightly and also helps stabilize the binding of DFHBI through polar contacts.[16] U31 of broccoli, which corresponds to U32 in baby spinach based on sequence alignment, also underwent very high levels of cleavage, suggesting that the same magnesium-dependent structure for binding DFHBI is also formed in the broccoli aptamer. Lead-induced cleavage was lower for U31 of broccoli, suggesting a less dynamic and more stable structure for broccoli around this nucleotide. By identifying the consensus sequence of spinach, baby spinach, and broccoli, we extrapolated the majority of the baby spinach aptamer

DOI: 10.1021/acschembio.6b00047
ACS Chem. Biol. XXXX, XXX, XXX−XXX

structure from the spinach crystal structure, except for part of the internal stem loop which is not present in the spinach crystal.[16,19] Overlaying the consensus and variable nucleotides of broccoli and baby spinach onto our extrapolated structure revealed where the differences between baby spinach and broccoli would likely lie within a structural context (Figure 1F). The only nucleotide that differed within the quadruplex core was A9 of baby spinach, corresponding to U8 of broccoli. Interestingly, A9 is extruded out of the spinach quadruplex core, is variable (replaced by a uridine in broccoli), and showed relatively strong lead-induced cleavage for broccoli. The accessibility to cleavage of U8 is in agreement with a predicted position on the periphery of the quadruplex core. Aside from A9/U8, all other variable nucleotides were in putative stem or stem-loop structures outside of the quadruplex-forming sequence. Together, these results indicate that broccoli and baby spinach are likely to possess very similar structures, including nearly identical quadruplex cores, and suggest that functional differences arise from quadruplex-flanking stem structures.

G-quadruplex structural stability is significantly enhanced in the presence of alkali metal ions, specifically potassium.[12] To further support the presence of a quadruplex structure in broccoli RNA and investigate the metal ion preferences of baby spinach and broccoli, we measured fluorescence activation of DFHBI-1T by each aptamer in the presence of 10 mM $MgCl_2$ or 50 mM of an alkali metal salt series: potassium (K^+), rubidium (Rb^+), sodium (Na^+), cesium (Cs^+), or lithium (Li^+) chloride. As controls, we used magnesium chloride alone and also tested the malachite green aptamer, which does not possess a quadruplex structure,[24] in the same salts and with its respective malachite green dye. Baby spinach showed strong fluorescence emission in the presence of K^+ ions but had a > 2-fold reduction in peak fluorescence with Rb^+ ions (Figure 2A). Virtually no fluorescence emission was observed in other salts. Broccoli fluorescence emission was higher than that of baby spinach in the presence of K^+ while Rb^+ also supported fluorescence quite well (Figure 2B). Sodium ions were also able to provide some degree of fluorescence emission, albeit at ~1/3 that of K^+ ions. Cesium, lithium, and magnesium alone supported little or no fluorescence of broccoli. Malachite green aptamer exhibited similar fluorescence emission spectra irrespective of the metal ions tested (Figure S1A). We performed titrations of KCl, NaCl, and LiCl and plotted the peak emission wavelength (507 nm) against salt concentration (Figure S1B,C). Baby spinach was found to respond to KCl with a 50% maximum fluorescence emission at about 10 mM (Figure S1B). However, no significant emission was detected in LiCl or NaCl up to 100 mM. In contrast, broccoli was nearly 2-fold more efficient in using K^+ ions with a KCl concentration of approximately 6 mM being sufficient to provide 50% maximum fluorescence emission (Figure S1C). Broccoli can also use sodium ions, but the concentration required for 50% maximum fluorescence was calculated to be over 200 mM.

G-quadruplexes uniquely coordinate potassium ions between stacked planar layers of guanine bases, which are formed by a combination of Watson−Crick and Hoogsteen base interactions.[25] Other ions of similar size and charge, such as rubidium and sodium, can sometimes also support quadruplex structure to a lesser extent.[12] In contrast, canonical Watson−Crick duplex structures usually have little preference for metal ion, which primarily act to neutralize negative phosphate backbone repulsions.[9,26] Likewise, cesium and lithium ions can sufficiently stabilize canonical nucleic acid helices by phosphate neutralization but do not stabilize G-quadruplexes very well.[12,27−29] Therefore, our results with various metal ions suggest that broccoli RNA possesses a G-quadruplex structure. The ability to activate fluorescence with sodium, however, demonstrates that broccoli's quadruplex is distinct from that of baby spinach. Because the predicted quadruplex-forming sequence is virtually unchanged between these two aptamers, flanking stem structures most likely influence alkali metal preferences by altering the local stability around the quadruplex.

To further correlate structure with function for the broccoli RNA aptamer and map critical nucleotides, we designed a systematic mutagenesis screen. DNA oligonucleotides containing a double-stranded T7 promoter sequence followed by single-stranded broccoli aptamer sequence were synthesized. This DNA template configuration is known to support efficient *in vitro* transcription by bacteriophage T7 RNA polymerase.[30] Every nucleotide position in the broccoli sequence was then systematically substituted with one of the three other nucleotide residues, generating almost 150 site-specific broccoli mutants. Rather than synthesize, purify, and test each broccoli mutant individually, we directly detected broccoli mutant fluorescence in real-time by including DFHBI-1T in transcription reactions and reading fluorescence over time in a quantitative PCR (qPCR) instrument.[31] This screening approach provided time-resolved readout of broccoli RNA mutant fluorescence as RNA molecules were synthesized (Figure 2C). Fluorescence can be directly correlated to broccoli RNA concentration by fitting relative fluorescence units to a standard curve (Figure S2A). The initial fluorescence from 4 to 8 min (F_0) and the maximum fluorescence values (F_{max}) observed over the course of the reaction were used to analyze the effect of each mutant on broccoli fluorescence activity. F_0 can be used as an approximate indicator of relative RNA folding, with presumably the fastest folding aptamers producing the greatest initial fluorescence. Once transcription has completed, broccoli RNA molecules with the greatest activation of fluorescence should provide the greatest F_{max} values, whereas those with substitutions at critical nucleotides would show reduced fluorescence.

Using this mutagenesis strategy, we screened all broccoli point mutants (Figure 2D). Aligning F_{max} values for all mutants together revealed several key features of broccoli RNA structure−function requirements. The initial discovery of broccoli suggested formation of a terminal stem and an internal stem loop structure but did not predict a quadruplex core nor how it would fold.[18] Our mutagenesis also supports the presence of the predicted stem structures. The first and last four nucleotides of broccoli could not be substituted successfully unless G:U wobble pairs were introduced (at positions 2, 4, 46, and 47), which then seemed to support a moderate degree of fluorescence. Positions 4 and 46 in particular responded well to mutation to a uridine, which would introduce a G:U or A-U pair, respectively, instead of an A:G purine−purine mismatch, to presumably stabilize the predicted terminal stem. The predicted internal stem also permitted moderate activity with similar mutations that converted A-U pairs to G:U pairs (at positions 16, 18, and 26), suggesting the presence of a Watson−Crick duplex. Near the center of the internal stem is a predicted loop with a consensus UUCG sequence shared between baby spinach and broccoli. Interestingly, UUCG is known to be a stabilizing sequence for loops,[32,33] which likely

DOI: 10.1021/acschembio.6b00047
ACS Chem. Biol. XXXX, XXX, XXX−XXX

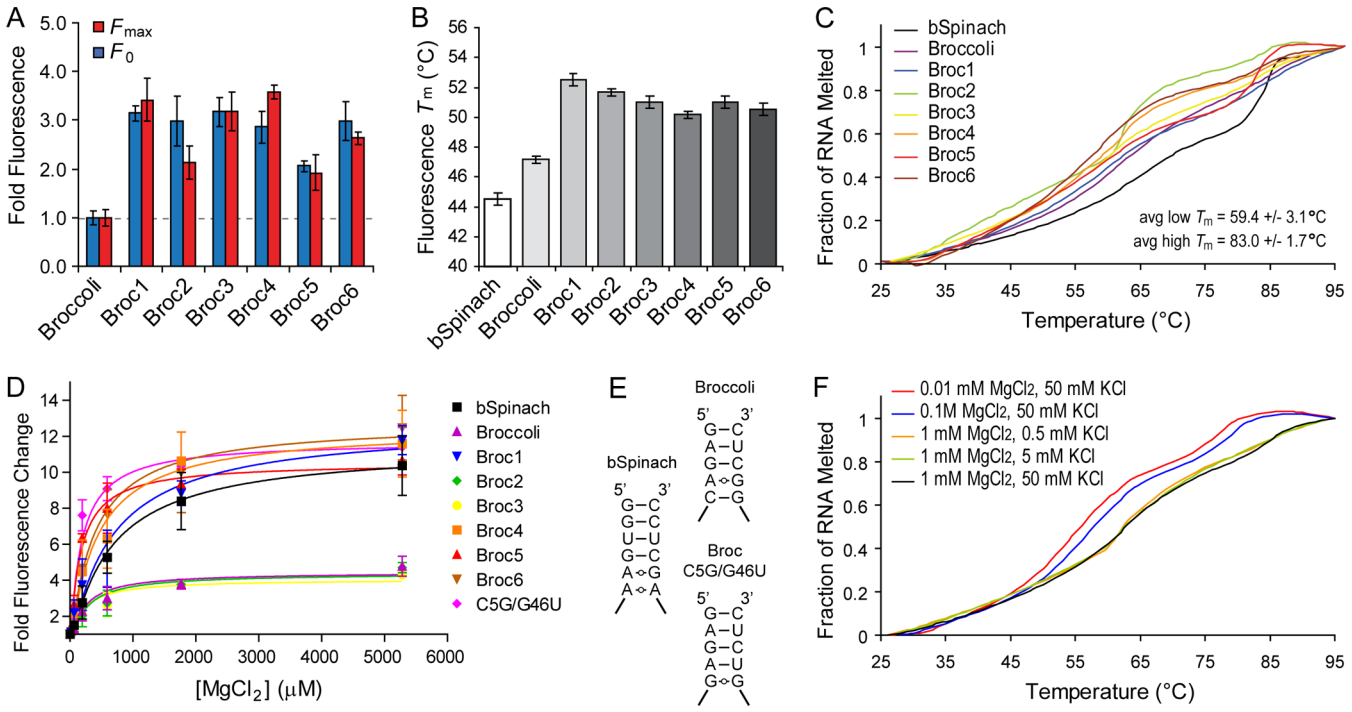

Figure 3. Sequence and structural variations in predicted quadruplex-flanking stem structures of broccoli RNA affect fluorescence, stability and magnesium-dependence. (A) Fluorescence activation of DFHBI-1T during *in vitro* transcription of broccoli mutants, referred to as Broc1 through Broc6. Normalized activity of control broccoli RNA fluorescence is indicated by a dashed gray line. Error is standard deviation. (B) Temperature-dependent fluorescence, defined as the temperature at 50% fluorescence activity, for Broc mutants. bspinach is baby spinach. Error bars are standard deviation. (C) Thermal denaturation of Broc mutants monitored by UV absorbance at 260 nm. Average melting temperature (T_m) values of the low or high temperature melt transitions are indicated. (D) Fluorescence of baby spinach (bspinach), broccoli, and Broc mutants during titration of $MgCl_2$. Peak emission (507 nm) is plotted against $MgCl_2$ concentration. C5G/G46U is a mutant of broccoli with sequence changes at base positions 5 and 46. Error bars are standard deviation. (E) Secondary structure illustrations of the terminal stem-to-quadruplex transitions of baby spinach, broccoli, and the C5G/G46U mutant. (F) Thermal denaturation of broccoli in buffered solutions with the indicated salts as monitored by UV absorbance at 260 nm.

explains its selection in the spinach aptamers.[15,16,18] However, this loop sequence was readily mutated while maintaining fluorescence that was similar to or better than regular broccoli. A recent systematic mutagenesis of spinach aptamer also found that mutation of the UUCG loop led to modulation of fluorescence and aptamer stability.[34] These results further support the formation of an internal stem loop.

Between the putative helical stem regions, numerous guanine residues exist that cannot be substituted without abolishing activity. These invariant guanine nucleotides suggest a direct role in quadruplex formation since no clear base-pairing interactions to cytosine or uridine nucleotides are apparent. Interspersed between invariant guanines, especially at the 3′ end, are several other residues that can be readily exchanged for other bases without suffering a severe loss of fluorescence. These residues may represent nucleotides bulged out of the quadruplex structure or otherwise involved in less critical hydrogen bonding or base stacking. These include nucleotides at positions 8, 32, 37, 39, 41, and 43. Based on the crystal structure of spinach and consensus sequence comparisons, all of these nucleotides except position 43 are extruded to the periphery of the quadruplex core and would be predicted to be less critical for quadruplex formation.[16,19] Certain mutations at some of these positions instead increased fluorescence activity, possibly due to improved stability through stacking or minimization of entropically costly solvent interactions.

Our mutagenesis screen also identified several mutants with substantially higher F_{max} values than the parent broccoli RNA. Arbitrary selection of 10 RNA transcription reactions from our mutagenesis screen followed by resolution on a denaturing polyacrylamide gel (Figure 2D) revealed similar levels of total RNA with no correlation to fluorescence activity, demonstrating that changes in fluorescence were not an artifact of different transcription efficiencies. Most of the enhanced fluorescence mutants were centered at the loop region of the putative stem loop. To investigate the general importance of the putative stem loop, we shortened the stem, deleted the loop, or deleted the entire stem loop (Figure S2B). All stem loop deletions significantly impaired or abolished fluorescence activity. Thus, broccoli fluorescence is very sensitive to changes in this stem loop region, in agreement with our site-specific mutations as well as previous mutagenesis by Filonov and co-workers.[18] These results indicate that the putative internal stem loop indeed plays an important role in mediating fluorophore activation.

On the basis of our initial mutagenesis, we generated a variety of combination mutants to further interrogate broccoli RNA structure and fluorescence. In our second round of mutagenesis, we combined several mutants, mostly in pairs (Figure S2C). Mutant names are simply listed as the position and the new nucleotide substituted at that position. Several mutations which seemed to enhance fluorescence were found to be incompatible with one another. These included combinatorial mutants containing 4U with 5G, 4U with 46U, and 43A with 46U, which presumably perturbed terminal stem formation or the transition from a duplex to quadruplex

DOI: 10.1021/acschembio.6b00047
ACS Chem. Biol. XXXX, XXX, XXX−XXX

structure when combined. Most combination mutants were designed to test compatibility of fluorescence-enhancing activity and revealed activity similar to or better than that of regular broccoli. The highest fluorescing mutants were again centered around the loop of the predicted internal stem loop. A third round of combinatorial mutagenesis identified several mutants with consistently higher fluorescence activity than regular broccoli (Figure S2D).

We selected four mutants and designed two new mutants to understand the basis of the apparent enhanced fluorescence. These six RNAs were named Broc1, Broc2, Broc3, Broc4, Broc5, and Broc6 (Figure S2E). The broccoli mutants exhibited 2−4-fold increases in F_0 or F_{max} during *in vitro* transcription in the presence of DFHBI-1T (Figure 3A). Thermal stability was considered a key limiting factor in the performance of the original spinach aptamer, which spurred mutagenesis to create spinach2.[7] To determine if thermal stability played a role in the enhanced fluorescence of our six selected broccoli mutants, we purified these RNAs and monitored fluorescence as temperature was increased. Taking the first derivative of the decrease in fluorescence, we estimated fluorescence-based melting temperature (T_m) values (Figure 3B). Baby spinach T_m was 44.5 °C, and broccoli T_m was approximately 47 °C, whereas Broc1−6 mutants ranged from 51 to 53 °C. Thus, all six Broc mutants exhibited a 4−6 °C increase in fluorescence-based thermal stability, which would be expected to improve fluorescence activity.

To obtain a closer look at thermal stability and RNA folding, we performed UV-monitored thermal denaturation studies with all six purified mutants in comparison to baby spinach and broccoli (Figure 3C). Three key points can be drawn from UV melt analyses. First, biphasic melt curves were observed to varying degrees for all aptamers. These results suggest at least a two-state folding model consistent with baby spinach and broccoli aptamers being composed of two relatively independent folding structures, which would include the predicted quadruplex and helical stem structures. Second, these aptamers displayed large variations in cooperative melting for the two structural states, indicating differences in the folding of the individual structures as well as the entire RNA. For example, Broc2 seems to fold the lower T_m structure with a more cooperative transition than the higher T_m structure. In contrast, Broc5 has the opposite profile where the higher T_m structure folds more cooperatively. Third, despite substantial changes in overall cooperativity of folding, the high and low T_m values calculated for all RNAs were similar, with ranges of ±3.1 °C at the lower T_m (59.4 °C average) and ±1.7 °C at the higher T_m (83.0 °C average; Figure S3A). These results suggest that the global structures of baby spinach, broccoli, and the Broc mutants are similar, which support out initial lead cleavage data, but that individually folding units with similar stabilities but different folding interactions exist. Melt profiles that are relatively linear, such as for regular broccoli, suggest a well-formed global structure with putative stem-to-quadruplex structures that fold and melt together. These thermal denaturation studies indicate that small but significant changes in the folding and stability of Broc1−6 may be associated with their apparent enhanced fluorescence.

To determine if metal ion preferences correlated with broccoli mutant fluorescence, we collected emission spectra in 50 mM of three different alkali metal ions, sodium (NaCl), rubidium (RbCl), or potassium (KCl). Fold change in fluorescence at the peak emission (507 nm) was plotted for each mutant in each salt condition (Figure S3B). Each mutant seemed to have similar fold increases in fluorescence when in the presence of potassium, and all were similar to or modestly better than broccoli. Broc2 and Broc3 were consistently similar to or better than broccoli for all metal ions tested.

Large enhancements in broccoli fluorescence from our mutagenesis screen were puzzling because broccoli was previously reported to be very efficient at fluorescence activation.[18] To rationalize our results, we considered that conditions in our transcription-based mutagenesis screen may be influencing fluorescence. Indeed, *in vitro* transcription reactions contained 40 mM $MgCl_2$, which would make it difficult to distinguish aptamer mutants with a magnesium dependence. A recent systematic mutagenesis to search for optimized spinach aptamers for *in vitro* applications also found enhanced aptamers in transcription reactions containing ∼20 mM $MgCl_2$.[35] However, the dependence of magnesium on aptamer function was not addressed. We considered that our mutagenesis screen results might help determine the basis for magnesium dependence among certain spinach family aptamers. We performed titrations of $MgCl_2$ with baby spinach, broccoli, and our six select Broc mutants (Figure 3D). We found a greater than 10-fold increase in fluorescence for baby spinach in the presence of high magnesium, while broccoli fluorescence increased less than 4-fold.

Among the Broc mutants, only Broc2 and Broc3 retained a low magnesium requirement like broccoli. Mutants Broc1, Broc4, Broc5, and Broc6 all exhibited a significant dependence on magnesium, similar to or greater than baby spinach. Upon inspection of the six Broc mutant sequences, we found that only Broc2 and Broc3 did not have a C5G and G46U mutation. When these two specific mutations were incorporated into parent broccoli to make a C5G/G46U mutant, magnesium-dependent fluorescence increased to over 10-fold mimicking the magnesium-dependence of baby spinach. This particular mutant had been screened during our combinatorial rounds of mutagenesis, and it showed increased fluorescence over broccoli (Figure S2C). In our initial screen, position C5 of broccoli could be converted to any base and still retained activity (Figure 2D). The proposed terminal stem of baby spinach and broccoli, based on the spinach crystal structure, shows noncanonical purine−purine pairs that are immediately adjacent to the quadruplex core (Figure 3E). These nucleotides and their pairing appear to directly influence magnesium binding or counterion effects and are likely to play a role in the stability of the stem-to-quadruplex transition. ispinach, a version of spinach recently optimized for *in vitro* applications, also retained these purine−purine pairs.[35] Thus, enhanced fluorescence of many of our mutants, in particular Broc1, -4, -5, and -6, could be relegated in part to a reliance on high magnesium for fluorescence. Importantly, all of the mutations for our six select Broc mutants were outside of the quadruplex region except for the A37U mutation, which is predicted to be extruded out of the quadruplex forming core based on our sequence and structural comparisons with spinach and baby spinach.

In support of magnesium-dependent stabilization of stem-to-quadruplex transitions, we performed UV thermal denaturation of broccoli in increasing magnesium or potassium concentrations. T_m values for both folding transitions increased as magnesium increased from 10 μM to 1 mM and the cooperativity of each transition became less pronounced. These results suggest that stem and quadruplex structures

DOI: 10.1021/acschembio.6b00047
ACS Chem. Biol. XXXX, XXX, XXX−XXX

fold independently without substantial magnesium, but in the presence of 1 mM magnesium their folding is more uniform, acting more like a single structure. Melting of broccoli in a constant 1 mM $MgCl_2$ but increasing KCl from 0.5 or 5 mM up to 50 mM revealed a change in the folding cooperativity of the more stable structure. In low KCl, the lower T_m structure did not change significantly, but a T_m value for the more stable structure could not be determined due to the lack of a clear transition. These results suggest that magnesium has a global effect on broccoli, most likely altering local stability and folding to improve transitions from stem to quadruplex structures. On the basis of these KCl-dependent effects, the more stable structure with a higher T_m value may correspond to a quadruplex while the less stable (lower T_m) structure may correspond to predicted stem structures.

Broccoli aptamers with mutations in quadruplex-flanking regions might translate to brighter or more stable fluorescence inside of cells. We cloned broccoli and the six select Broc mutants into bacterial expression vectors. Broccoli sequences were flanked by a T7 promoter and a T7 terminator without a scaffold sequence (ie, no tRNA scaffold) and transformed into Rosetta (DE3) *E. coli* cells. After induction of broccoli RNA expression, cells were incubated with DFHBI-1T and fluorescence measured. Compared to broccoli, Broc3 had the highest fluorescence by about 1.6 fold (Figure S3D). Comparing broccoli and Broc3 binding affinity to DFHBI-1T did not reveal any significant differences in the calculated K_d values (Figure S3E). On the basis of the small increase in potassium utilization, a T_m increase of a few degrees, similar magnesium dependence, and similar DFHBI-1T binding affinity, the modest improvement of Broc3 fluorescence over broccoli in *E. coli* seems reasonable. However, a direct correlation between *in vivo* and *in vitro* fluorescence for the tested Broc mutants was not clear, indicating that multiple factors contribute to effective fluorescence inside of cells and highlighting the need to optimize RNA scaffolds for *in vivo* applications.[36]

Effectively developing, optimizing, and using fluorescent RNA aptamers requires understanding of the principles of RNA structure that support successful fluorophore binding or activation. Such studies are expected to eventually contribute to the development of reliable, multicolored fluorescent RNA tool kits for molecular and chemical biology applications. Our results indicate that broccoli is a G-quadruplex-containing RNA with a structure that is very similar to that of baby spinach and spinach. Duplex stem structures that flank the central quadruplex structure alter the stability, metal ion preferences and fluorescence activity of baby spinach and broccoli. In particular, the transitions from stem to quadruplex are proposed to play a significant role in magnesium dependence of these GFP-mimic RNAs and is an important target for optimizing their stability and metal ion preferences. The role of magnesium in stabilizing tertiary RNA structures around transitions of independently folding units has been recognized previously, such as for pseudoknots, three-helix junctions, and tRNA folding.[37−39] Magnesium appears to aid in formation of a more uniform aptamer by improving the cooperativity of folding between stem and quadruplex structures in broccoli. Therefore, spinach derivatives likely exhibit diverse requirements for magnesium depending on their ability to achieve sufficiently favorable stem-to-quadruplex transitions. A systematic mutagenesis of the first generation spinach aptamer recently reported that purine−purine pairing at the terminal stem-to-quadruplex transition had important effects on thermodynamic stability and fluorescence activity.[34] These are the same purine−purine pairs that we have shown to modulate magnesium dependence. Analyses of DNA duplex-to-quadruplex transitions have also highlighted the importance of noncanonical pairing to accommodate stable transitions.[40] Thus, designing and optimizing better aptamers, such as RNA mimics of GFP, should take into consideration the interactions and transitions between independently folding structural elements and the role of metal ions in stabilizing them.

METHODS

RNA Synthesis. RNA was synthesized by T7 *in vitro* transcription starting with DNA templates purchased from Integrated DNA Technologies (IDT). Single-stranded DNA templates were annealed to a T7 promoter oligo (TAATACGACTCACTATA) to generate double-stranded promoter regions, which support *in vitro* transcription by T7 RNA polymerase.[30] T7-DNA template and synthesized RNA sequences for all mutants are listed in Table S1. *In vitro* transcription was performed by standard protocols. Briefly, reactions contained purified T7 RNA polymerase, 30 mM Tris (at pH 7.9), 12.5 mM NaCl, 40 mM $MgCl_2$, 2% PEG_{8000}, 0.05% Triton-X 100, 2 mM spermidine, and 2.5 μM T7-DNA template. Afterward, the DNA template was degraded by the addition of 1 unit of DNase I for every 20 μL of reaction and incubated at 37 °C for 15 min. Reactions were phenol-chloroform extracted and gel-purified from denaturing polyacrylamide gels. Purified RNA was quantified by measuring absorbance at 260 nm and calculated extinction coefficients using nearest neighbor approximations and Beer's Law.

RNA Structure Probing by Lead Acetate Cleavage. Lead cleavage mapping was performed similar to published protocols.[20] The 5′ phosphates of 100 pmol of *in vitro* transcribed baby spinach and broccoli RNA were removed by treatment with alkaline phosphatase. Dephosphorylated RNA was radiolabeled with [γ-^{32}P]-ATP and T4 polynucleotide kinase then gel-purified. A total of 60 000 cpm of radiolabeled RNA (~2 pmol) was refolded by heating to 95 °C and cooling to 23 °C in 20 mM Tris (at pH 7.2), 5 mM $MgCl_2$, 0.2% DMSO, 1 mg mL^{-1} tRNA, 50 mM CsCl or KCl, and with or without 20 μM DFHBI-1T (Lucerna Technologies). Freshly prepared lead acetate was then added to a final of 2 mM, and the reaction was incubated at 23 °C for 20 min before being precipitated by the addition of 10 vols of 2% $LiClO_4$ in acetone. Alkaline hydrolysis ladders were prepared by incubation of radiolabeled RNA at 90 °C for 8 min in 20 mM $NaHCO_3$ (pH 10), 1 mM EDTA, and 1 mg mL^{-1} tRNA then precipitated with 2% $LiClO_4$ in acetone. T1 RNase ladders were prepared by incubation of radiolabeled RNA with 1 U of T1 RNase at 23 °C for 10 min in 25 mM phosphate buffer (pH 7.0), 150 mM NaCl, 1 mM $MgCl_2$, 0.2 mM EDTA, and 1 mg mL^{-1} tRNA then precipitated with 2% $LiClO_4$ in acetone. Precipitated reactions were washed with acetone, boiled in 90% formamide, 1× TBE, then resolved on a 15% denaturing polyacrylamide sequencing gel. Gels were dried and exposed to phosphorimager to visualize radioactive RNA bands.

Fluorescence Spectra, Salt Titrations, and DFHBI-1T Binding Affinity. Purified RNA was refolded by heating to 95 °C for 3 min then slow cooling to RT at a rate of approximately 1 °C/min in the following reaction: 20 mM cacodylate (pH 7.2), 1 mM $MgCl_2$, 0.05% DMSO, and 5 μM DFHBI-1T. RNA was included at 0.5 μM and XCl (X = K, Rb, Na, Li, or Cs) at 50 mM. For salt titrations, small volumes of 2 M salt solutions were added to 400 μL reactions and incubated at RT for 3 min, then emission spectra were collected. Fluorescence values were corrected for increased volume of each reaction over the course of titration. Fold fluorescence change was calculated by dividing the fluorescence value after each salt addition by the initial value before the addition of the titrated salt. For determining the binding affinity of broccoli and Broc3 RNA for DFHBI-1T, increasing concentrations of each RNA were refolded in the above-noted reaction buffer except

DOI: 10.1021/acschembio.6b00047
ACS Chem. Biol. XXXX, XXX, XXX−XXX

with 100 nM of DFHBI-1T. Excitation and emission spectra for these assays were collected on a Horiba Fluorolog-3 spectrofluorometer. Peak emission at 507 nm was plotted against salt concentration. All experiments were performed in duplicate or triplicate and curves fit by nonlinear regression in Prism (Graphpad).

Systematic Broccoli Aptamer Mutagenesis Monitored by Fluorescence. To perform systematic mutagenesis of broccoli RNA, we combined *in vitro* transcription with real time fluorescence readout using a BioRad CFX96 quantitative PCR machine. This approach was inspired by a similar technique described by Jaschke and co-workers.[31] Single-stranded broccoli mutant T7-DNA templates were purchased from IDT in 96-well plates normalized to 2 nmol of DNA. These single DNA strands represented the antisense sequence. To each well, 40 μL of resuspension buffer was added (5 mM Tris, pH 7.0, 0.1 mM EDTA) and 40 μL of T7 promoter oligo (sense sequence) at 50 μM in water, for a final of 25 μM template. To ensure efficient annealing of the T7 promoter oligo, plates were sealed and incubated at 80 °C for 10 min, then slow cooled to RT, spun down, and gently vortexed. For transcription reactions, 1 μL of each template was spotted into new 96-well plates followed by the addition of 9 μL of ice-cold transcription reaction mix on ice. The standard transcription reaction described above was used; however KCl was added to a final of 3 mM and DFHBI-1T to 60 μM. Reactions also contained 12.5 mM NaCl from the T7 RNA polymerase storage buffer. To initiate reactions, plates were placed into a BioRad CFX96 block set at 4 °C. The block was then cycled to 37 °C and held for 1 h. The plate was read using all channels (which includes the FAM/SYBR filter) once at 4 °C then every 1 min and 48 s (reading takes 12 s) at 37 °C such that fluorescence reading was at 2 min intervals. Data were exported to Excel for analysis. Maximum fluorescence values over a 1 h time course were used for comparing mutants. Initial fluorescence, defined as the change in fluorescence over the change in time from 4 to 8 min, was also used for comparing mutant performance. Four or more separate experiments were performed for each screen, and error was calculated by standard deviation.

Fluorescence-Based Determination of RNA Melting Temperature. To determine temperature dependence of fluorescence, purified broccoli RNAs at 10 μM were refolded in 20 mM cacodylate (pH 7.2), 50 mM KCl, 1 mM $MgCl_2$, and 20 μM DFHBI-1T by heating to 95 °C for 3 min then slow cooling to RT. Reactions were placed in 96-well plates in a BioRad CFX96 and a typical qPCR melt analysis was performed. Reactions were heated from 25 to 95 °C at 0.5 °C increments. Reactions were held at each temperature for 30 s before plate reading. BioRad software on the CFX96 automatically determined the derivative of the melt curve and autocalculated T_m values.

Thermal Denaturation of RNA Monitored by UV Absorbance. RNA reactions were prepared as described for fluorescence-based T_m determination, but only 1 μM RNA and 5 μM DFHBI-1T were used. Degassed water was used to prepare samples. Data were collected in a Cary 400 UV/vis spectrophotometer. Reactions were heated to 95 °C then slow cooled at 1 °C/min. Samples were then heated and cooled from 25 to 95 °C three times at a ramp rate of 1 °C/min, while UV absorbance was collected every 1 min. Melting temperatures were determined using Van't Hoff calculations on up ramps only (dissociation curves) and error determined by standard deviation.

Expression and Fluorescence Measurement of Broccoli RNA in *E. coli*. Double-stranded DNA sequences encoding broccoli and broccoli mutants were synthesized by IDT and cloned into a pIDT-SMART vector (ampicillin resistant) containing a custom multiple cloning site. The broccoli sequences were inserted 30 bases downstream from a T7 promoter and 10 bases upstream of a T7 terminator. After sequencing to confirm cloning, plasmids were transformed into Rosetta (DE3) cells and grown at 37 °C with shaking. Cultures were measured by absorbance at 600 nm and normalized to an A_{600} of 0.5. IPTG was then added to a final of 0.5 mM and DFHBI-1T to a final of 10 μM, and shaking continued at 37 °C for 4 h. Cells were harvested, spun down, and resuspended in 400 μL of PBS and their absorbance at 600 nm checked again and adjusted to match, then DFHBI-1T was added to 10 μM and incubated on ice for 30 min. A total of 100 μL of each sample was spotted into four wells of a black 96-well fluorescence plate. Reactions were then read in a Promega GloMax plate reader three times using a green fluorescence filter set. Raw fluorescence was normalized and plotted. Error was calculated as standard deviation from three independent experiments.

■ ASSOCIATED CONTENT

Supporting Information

The Supporting Information is available free of charge on the ACS Publications website at DOI: 10.1021/acschembio.6b00047.

Fluorescence of malachite green, baby spinach, and broccoli RNA aptamers in alkali metal salts; fluorescence of broccoli aptamer stem-loop mutants and rounds 2−4 of site-specific mutagenesis; UV melts of broccoli and Broc1−6 mutants, fluorescence of Broc1−6 mutants in *E. coli*, binding affinity of broccoli and Broc3 to DFHBI-1T (PDF)

Table S1: Oligonucleotide Sequences (XLS)

■ AUTHOR INFORMATION

Corresponding Author

*E-mail: ktgagnon@siu.edu.

Author Contributions

§These authors contributed equally.

Notes

The authors declare no competing financial interest.

■ ACKNOWLEDGMENTS

We thank M. McCarroll for access to a Horiba Fluorolog spectrofluorometer and the R. Gupta laboratory for insightful discussions. This work was supported by a Team Development Grant from Southern Illinois University to K.T.G. and an ALS Association grant to K.T.G (16-IIP-260).

■ REFERENCES

(1) Feigon, J., Dieckmann, T., and Smith, F. W. (1996) Aptamer structures from A to zeta. *Chem. Biol. 3*, 611−617.

(2) Tuerk, C., and Gold, L. (1990) Systematic evolution of ligands by exponential enrichment: RNA ligands to bacteriophage T4 DNA polymerase. *Science 249*, 505−510.

(3) You, M., Litke, J. L., and Jaffrey, S. R. (2015) Imaging metabolite dynamics in living cells using a spinach-based riboswitch. *Proc. Natl. Acad. Sci. U. S. A. 112*, E2756−2765.

(4) You, M., and Jaffrey, S. R. (2015) Designing optogenetically controlled RNA for regulating biological systems. *Ann. N. Y. Acad. Sci. 1352*, 13−19.

(5) Rogers, T. A., Andrews, G. E., Jaeger, L., and Grabow, W. W. (2015) Fluorescent monitoring of RNA assembly and processing using the split-spinach aptamer. *ACS Synth. Biol. 4*, 162−166.

(6) Arora, A., Sunbul, M., and Jaschke, A. (2015) Dual-colour imaging of RNAs using quencher- and fluorophore-binding aptamers. *Nucleic Acids Res. 43*, e144.

(7) Strack, R. L., Disney, M. D., and Jaffrey, S. R. (2013) A superfolding spinach2 reveals the dynamic nature of trinucleotide repeat-containing RNA. *Nat. Methods 10*, 1219−1224.

(8) Dolgosheina, E. V., Jeng, S. C., Panchapakesan, S. S., Cojocaru, R., Chen, P. S., Wilson, P. D., Hawkins, N., Wiggins, P. A., and Unrau, P. J. (2014) RNA mango aptamer-fluorophore: a bright, high-affinity complex for RNA labeling and tracking. *ACS Chem. Biol. 9*, 2412−2420.

(9) Tan, Z. J., and Chen, S. J. (2011) Importance of diffuse metal ion binding to RNA. *Met. Ions Life Sci. 9*, 101−124.

DOI: 10.1021/acschembio.6b00047
ACS Chem. Biol. XXXX, XXX, XXX−XXX

(10) Pyle, A. M. (2002) Metal ions in the structure and function of RNA. *JBIC, J. Biol. Inorg. Chem. 7*, 679−690.
(11) Auffinger, P., D'Ascenzo, L., and Ennifar, E. (2016) Sodium and Potassium Interactions with Nucleic Acids. *Met. Ions Life Sci. 16*, 167−201.
(12) Largy, E., Mergny, J. L., and Gabelica, V. (2016) Role of Alkali Metal Ions in G-Quadruplex Nucleic Acid Structure and Stability. *Met. Ions Life Sci. 16*, 203−258.
(13) You, M., and Jaffrey, S. R. (2015) Structure and Mechanism of RNA Mimics of Green Fluorescent Protein. *Annu. Rev. Biophys. 44*, 187−206.
(14) Babendure, J. R., Adams, S. R., and Tsien, R. Y. (2003) Aptamers switch on fluorescence of triphenylmethane dyes. *J. Am. Chem. Soc. 125*, 14716−14717.
(15) Paige, J. S., Wu, K. Y., and Jaffrey, S. R. (2011) RNA mimics of green fluorescent protein. *Science 333*, 642−646.
(16) Warner, K. D., Chen, M. C., Song, W., Strack, R. L., Thorn, A., Jaffrey, S. R., and Ferre-D'Amare, A. R. (2014) Structural basis for activity of highly efficient RNA mimics of green fluorescent protein. *Nat. Struct. Mol. Biol. 21*, 658−663.
(17) Song, W., Strack, R. L., Svensen, N., and Jaffrey, S. R. (2014) Plug-and-play fluorophores extend the spectral properties of spinach. *J. Am. Chem. Soc. 136*, 1198−1201.
(18) Filonov, G. S., Moon, J. D., Svensen, N., and Jaffrey, S. R. (2014) broccoli: rapid selection of an RNA mimic of green fluorescent protein by fluorescence-based selection and directed evolution. *J. Am. Chem. Soc. 136*, 16299−16308.
(19) Huang, H., Suslov, N. B., Li, N. S., Shelke, S. A., Evans, M. E., Koldobskaya, Y., Rice, P. A., and Piccirilli, J. A. (2014) A G-quadruplex-containing RNA activates fluorescence in a GFP-like fluorophore. *Nat. Chem. Biol. 10*, 686−691.
(20) Gagnon, K. T., and Maxwell, E. S. (2015) Assessing intermolecular RNA:RNA interactions within a ribonucleoprotein complex using heavy metal cleavage mapping. *Methods Mol. Biol. 1240*, 125−134.
(21) Brown, R. S., Dewan, J. C., and Klug, A. (1985) Crystallographic and biochemical investigation of the lead(II)-catalyzed hydrolysis of yeast phenylalanine tRNA. *Biochemistry 24*, 4785−4801.
(22) Pan, T. (2000) Probing RNA structure by lead cleavage, *Curr. Protoc. Nucleic Acid Chem.* Chapter 6, Unit 6 3, p 6.3.1, John Wiley & Sons, Inc., Hoboken, NJ, DOI: 10.1002/0471142700.nc0603s00.
(23) Markley, J. C., Godde, F., and Sigurdsson, S. T. (2001) Identification and characterization of a divalent metal ion-dependent cleavage site in the hammerhead ribozyme. *Biochemistry 40*, 13849−13856.
(24) Baugh, C., Grate, D., and Wilson, C. (2000) 2.8 A crystal structure of the malachite green aptamer. *J. Mol. Biol. 301*, 117−128.
(25) Campbell, N. H., and Neidle, S. (2012) G-quadruplexes and metal ions. *Met. Ions Life Sci. 10*, 119−134.
(26) Dammertz, K., Hengesbach, M., Helm, M., Nienhaus, G. U., and Kobitski, A. Y. (2011) Single-molecule FRET studies of counterion effects on the free energy landscape of human mitochondrial lysine tRNA. *Biochemistry 50*, 3107−3115.
(27) Kim, B. G., Evans, H. M., Dubins, D. N., and Chalikian, T. V. (2015) Effects of Salt on the Stability of a G-Quadruplex from the Human c-MYC Promoter. *Biochemistry 54*, 3420−3430.
(28) Marincola, F. C., Virno, A., Randazzo, A., and Lai, A. (2007) Effect of rubidium and cesium ions on the dimeric quaduplex formed by the Oxytricha nova telomeric repeat oligonucleotide d-(GGGGTTTTGGGG). *Nucleosides, Nucleotides Nucleic Acids 26*, 1129−1132.
(29) Creze, C., Rinaldi, B., Haser, R., Bouvet, P., and Gouet, P. (2007) Structure of a d(TGGGGT) quadruplex crystallized in the presence of Li+ ions. *Acta Crystallogr., Sect. D: Biol. Crystallogr. 63*, 682−688.
(30) Milligan, J. F., Groebe, D. R., Witherell, G. W., and Uhlenbeck, O. C. (1987) Oligoribonucleotide synthesis using T7 RNA polymerase and synthetic DNA templates. *Nucleic Acids Res. 15*, 8783−8798.
(31) Hofer, K., Langejurgen, L. V., and Jaschke, A. (2013) Universal aptamer-based real-time monitoring of enzymatic RNA synthesis. *J. Am. Chem. Soc. 135*, 13692−13694.
(32) Heus, H. A., and Pardi, A. (1991) Structural features that give rise to the unusual stability of RNA hairpins containing GNRA loops. *Science 253*, 191−194.
(33) Dichtl, B., Pan, T., DiRenzo, A. B., and Uhlenbeck, O. C. (1993) Replacement of RNA hairpins by in vitro selected tetranucleotides. *Nucleic Acids Res. 21*, 531−535.
(34) Ketterer, S., Fuchs, D., Weber, W., and Meier, M. (2015) Systematic reconstruction of binding and stability landscapes of the fluorogenic aptamer spinach. *Nucleic Acids Res. 43*, 9564−9572.
(35) Autour, A., Westhof, E., and Ryckelynck, M. (2016) ispinach: a fluorogenic RNA aptamer optimized for in vitro applications. *Nucleic Acids Res. 44*, 2491−2500.
(36) Filonov, G. S., Kam, C. W., Song, W., and Jaffrey, S. R. (2015) In-gel imaging of RNA processing using broccoli reveals optimal aptamer expression strategies. *Chem. Biol. 22*, 649−660.
(37) Quigley, G. J., Teeter, M. M., and Rich, A. (1978) Structural analysis of spermine and magnesium ion binding to yeast phenylalanine transfer RNA. *Proc. Natl. Acad. Sci. U. S. A. 75*, 64−68.
(38) Soto, A. M., Misra, V., and Draper, D. E. (2007) Tertiary structure of an RNA pseudoknot is stabilized by "diffuse" Mg2+ ions. *Biochemistry 46*, 2973−2983.
(39) Noeske, J., Schwalbe, H., and Wohnert, J. (2007) Metal-ion binding and metal-ion induced folding of the adenine-sensing riboswitch aptamer domain. *Nucleic Acids Res. 35*, 5262−5273.
(40) Lim, K. W., and Phan, A. T. (2013) Structural basis of DNA quadruplex-duplex junction formation. *Angew. Chem., Int. Ed. 52*, 8566−8569.

DOI: 10.1021/acschembio.6b00047
ACS Chem. Biol. XXXX, XXX, XXX−XXX